LA-UR-03-4452

Title: MEASUREMENT OF FIBER-SCALE RESIDUAL STRESSES IN A METAL MATRIX COMPOSITE

Author(s): Michael B Prime (ESA-WR)
Michael R. Hill (U. C. Davis)

Submitted to: Journal of Composite Materials

Measurement of Fiber-Scale Residual Stress Variation in a Metal Matrix Composite

Michael B. Prime
Engineering Sciences and Applications Division
Los Alamos National Laboratory
Los Alamos, NM 87545 USA
prime@lanl.gov

Michael R. Hill
Mechanical and Aeronautical Engineering Department
University of California
Davis, CA, 95616 USA

Revision 1 Accepted April 2004 to *Journal of Composite Materials*

ABSTRACT

The crack compliance, or slitting, method was used to measure a localized depth profile of residual stresses in a metal matrix composite. The composite consisted of a matrix of Kanthal, a Fe-Cr-Al refractory alloy, reinforced with continuous uniaxial tungsten fibers. The stress measurements involved successively deepening a narrow slit between fibers in the matrix, and measuring the resulting deformations with a surface strain gage. The depth profile of the in-plane residual stress components was determined from the measured strains using an eigenstrain-based extension of the residual stress calculation scheme normally used for slitting measurements. To validate some of the eigenstrain assumptions, the measured residual stresses were compared with predictions from a thermomechanical finite element model. The model used a mesh of the actual fiber arrangement in the composite specimen rather than the commonly used unit cell model. Compared to other techniques for measuring residual stresses in composites, the slitting measurements provided spatial resolution to a small fraction of the fiber diameter, which is useful when validating a thermomechanical model. Coincidentally, this is the first reported slitting method measurement of shear residual stresses.

INTRODUCTION

Residual stresses play a significant role in failures of composite materials. The most common example is that fiber-matrix debonding and pullout are significantly affected by the residual stress normal to the fiber-matrix interface [1,2,3]. Other performance characteristics have also been found to be affected by residual stress, including matrix cracking [4], yield strength [5,6], and dimensional stability [7]. It is therefore important to develop methods for the measurement and prediction of residual stresses in composite materials. This paper mainly presents measurements of the spatial distribution of residual stress in a metal matrix composite but also compares the measured stresses to predictions from a thermomechanical simulation.

The specific residual stresses that contribute to matrix-fiber failures are difficult to measure with sufficient spatial resolution to predict their effects. Local stresses cause failures, e. g., the residual stresses precisely at the matrix-fiber interface, but most methods measure spatially averaged stresses. Neutron diffraction, for example, can distinguish between reinforcement and matrix stresses, but usually only gives values that are spatially averaged over large volumes [e.g., 8]. Several other techniques can measure residual stresses on the scale of individual plies in a laminate but still not at the scale of the fibers [9,10]. The inability to measure local values of residual stresses can also lead to difficulties in validating models for residual stress prediction because a spatially averaged stress is not unique to a distribution of local stresses; hence a prediction of local stresses cannot be uniquely validated. In their extensive review on residual stresses, Withers and Bhadeshia [11] state that for composites "it is difficult to obtain validatory stress measurements due to insufficient spatial resolution of the measurement techniques for all but the coarsest systems." The only reported measurements of residual stress variations at the fiber scale come from synchrotron x-ray measurements [12,13]. However, such measurements require crystalline materials and access to a synchrotron source and are not always feasible.

This work reports an application of the crack compliance, or slitting, method to determine a spatially refined local stress distribution in a uniaxial continuous-fiber reinforced composite. The local stresses were determined at a spatial resolution on the scale of a fraction of the minimum dimension of the reinforcement phase (i.e., the fiber diameter). Previous applications of the slitting method to reinforced composites have examined residual stress variations on larger scales. An application to particulate-reinforced composites treated the composite as a homogeneous isotropic continuum [14]. Slitting has also been applied to composites with a limited number of material regions such as a functionally graded material

with seven discrete regions [15], multi-layer graphite epoxy composites where each layer was treated as an orthotropic continuum [16,17], and a Ti/SiC unidirectional composite panel with unreinforced cladded layers [18]. In all of these applications the measured stresses were macroscopic averages of the matrix and reinforcement stresses.

MATERIAL

Tungsten fiber-reinforced Kanthal metal matrix is a model system developed through collaboration between NASA's Lewis Research Center and Tufts University, Massachusetts, to explore performance in applications where high strength is desired at high temperatures (1300 - 1700 K) [19]. In particular, the use of continuous fibers offers superior high-temperature stability compared to discontinuous fiber composites. The matrix alloy, Kanthal, belongs to a family of Fe-Cr-Al refractory alloys that exhibit outstanding high-temperature oxidation resistance, mechanical behavior, and weldability. For example, the yield stress is reported to be 275 MPa at 806 K [20]. Potential applications for the composite include corrosion resistant cladding or reactor fuel containment in space nuclear systems. To enhance Kanthal's strength, tungsten fibers are added, which have a high melting temperature (3660 K) and negligible creep below around 1273 K [21]. The disadvantage is the development of residual stress because of the mismatch in the coefficient of thermal expansion between the Kanthal (9.58 x 10^{-6}/K) and the tungsten (4.4 x 10^{-6}/K) during cooling from fabrication temperatures of around 1338 K.

Tungsten/Kanthal composites containing nominally 10, 20, 30, and 70 % volume fraction (V_f) GE 218 tungsten fibers (diameter ≈ 200 μm) were fabricated at NASA Lewis Research Center using the arc-spray method. The Kanthal matrix composition in weight-percent is 73.2 Fe, 21 Cr, 5.8 Al, and 0.04 C. Tapes containing unidirectional fibers were hot pressed at 1338 K for 1 hour before being slowly cooled to room temperature. The as-fabricated bars were approximately 25 mm wide, 2.5 mm thick, and 200 mm long. An additional monolithic Kanthal bar was fabricated and taken through the same heating cycle. Only the nominally 10 % V_f specimen was measured in this study. Examination of a cross-section of the specimen after the study revealed the true fiber volume fraction to be about 8.5 %.

SLITTING EXPERIMENT

The residual stresses were measured in the 8.5 % V_f specimen and in a monolithic specimen using an extension to the slitting method [22]. The test arrangement is shown in Figure 1. A 120 ohm resistance strain gage with a 381 μm active gage length was mounted on the top of the specimen using epoxy. After mounting, the gage was waterproofed using polyurethane. Two considerations guided the placement of the strain gage. First, the slit was to be cut between two of the fibers on the row nearest to the free surface of the specimen. Such positioning with respect to the fibers was achieved by examining the side of the specimen to locate the fibers and then marking the fiber locations on the top of the specimen (assuming the fibers were straight). Second, the gage had to be as close as possible to the slit to get maximum sensitivity of the strain readings. Some of the plastic gage backing was trimmed away so that the slit could be made very close to the active element of the gage. However, electric discharge machining cannot cut through non-conductive material like adhesive or polyurethane, especially with a small wire. Therefore, the proximity of the gage to the slit was limited by the need to have space between the slit where the adhesive could extend beyond the gage and where the polyurethane could then overlap the adhesive.

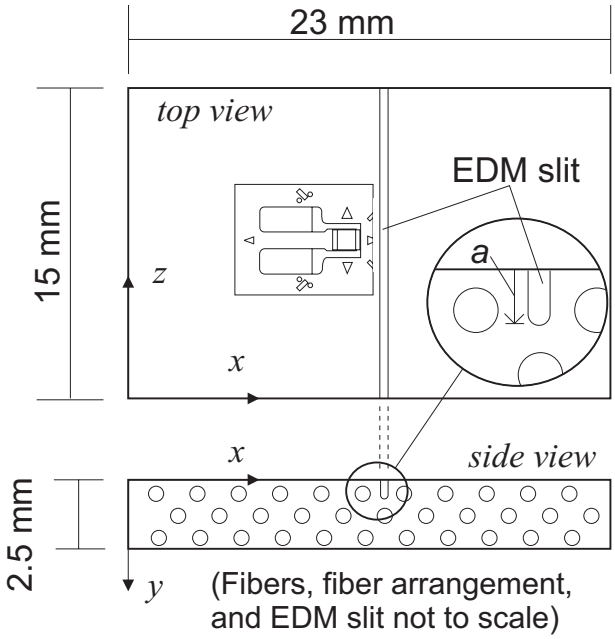

Figure 1. Location of strain gage and EDM slit on composite specimen used for residual stress measurement.

A 30 μm diameter tungsten wire cut a slit 80 μm wide (Fig 2) by wire electric discharge machining (EDM). The use of such a small wire for slitting measurements, necessary here in order to cut between the fibers, has only been reported in the literature once before [23]. The wire axis was oriented parallel to the fibers during cutting (i.e., along the *z*-direction). The slit was cut in 25 μm increments of depth (*y*-direction), releasing the residual stresses on the plane of the slit (σ_x and τ_{xy}). Strains (ε_x) caused by stress release were measured using the strain gauge on the top surface after each increment. The EDM cutting was performed at low power while the specimen was submerged in temperature-controlled deionized water so that no noticeable thermal stresses were induced during the process. After the test, the distance from the edge of the slit (nearest the strain gage) to the center of the strain gage grid was measured, as was the final slit depth, using a microscope with an instrumented two-axis stage. Such

measurement of the actual geometry is crucial for obtaining accurate results [24].

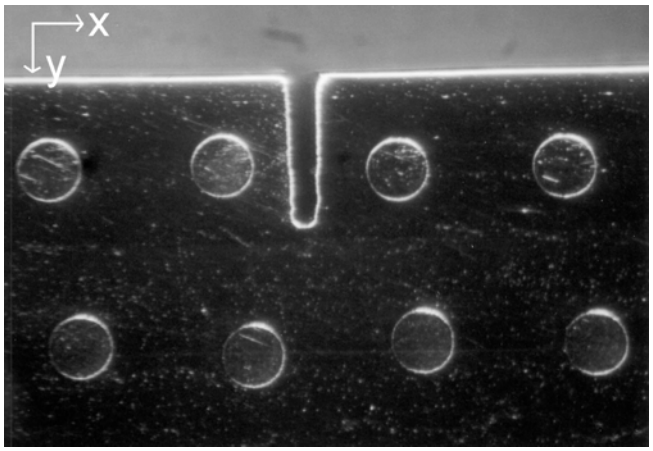

Figure 2. Micrograph showing final depth of slit cut by wire EDM in the metal matrix composite. Fibers are 200 μm diameter.

DATA ANALYSIS

Key assumptions normally made when applying the slitting method were employed here to compute residual stress from measured strain versus depth data. First, the specimen was assumed to behave elastically during the slitting experiment, which is generally valid for low levels of residual stress. Second, based on earlier work [25], the wire EDM cutting process was assumed to not introduce residual stresses.

To admit the possibility of non-zero shear stress (τ_{xy}) on the slit plane in the composite specimen, an alternate approach to the data reduction was adopted. The slitting method normally relies on an insignificant level of shear stress on the slit plane, and in that case the single residual stress component normal to the slit plane (here $\sigma_x(y)$) is found from the measured strains using a series expansion for $\sigma_x(y)$ [22,26]. Because the level of shear stress on the slit plane in this application is not necessarily negligible, it was necessary to formulate the stress computation differently. Using the conventional series expansion approach, it would not be possible to uniquely determine $\sigma_x(y)$ and $\tau_{xy}(y)$ using only data from a single strain gage. Because the specimen was long and uniform in the *z*-direction the stresses away from the ends can be assumed to be uniform. Therefore, the other shear stress, τ_{xz}, that could be released by the cut was assumed to be zero. Even if it were non-zero, that shear-stress component would have negligible effect on the normal strain measured by the gage.

In this work, residual stresses are found by assuming that $\sigma_x(y)$ and $\tau_{xy}(y)$ are physically related rather than independent. This is accomplished for the composite by first determining a distribution of misfit strain from the slitting strains, as an intermediate step to determining residual stresses. The misfit strain tensor ε_{kl}^* enters the elasticity problem through the constitutive relation

$$\sigma_{ij} = D_{ijkl}(\varepsilon_{kl} - \varepsilon_{kl}^*) \qquad (1)$$

where σ_{ij} and D_{ijkl} are the stress and elastic constitutive tensors normally appearing in elasticity, ε_{kl} is the total strain, and (ε_{kl} -ε_{kl}^*) is the elastic strain. This approach to finding residual stress relies on finding the misfit strain field from elastic strain release due to sectioning (rather than on finding residual stress directly), and the method has been pursued previously for measuring weld residual stresses (i.e., the inherent strain approach of Ueda, et al [27] and the eigenstrain approach of Hill, et al [28, 29]). We will refer to ε_{kl}^* as "eigenstrain", adopting the term used previously by Mura [30]. Once the distribution of eigenstrain is determined, residual stress is computed by an elastic initial strain calculation.

In the present experiment, the situation is simple enough to motivate physically based assumptions regarding the character and distribution of the eigenstrain, and these significantly simplify determining the eigenstrain (and residual stress) distribution. The slit plane was cut near the center (*x*-direction) of the specimen and strains were measured at the middle (*z*-direction) of the slit length. Since material response near the middle of the specimen during hot pressing and subsequent cooling was likely independent of the fiber direction (*z*), we assume an eigenstrain field independent of *z*. Since deformation during cooling is normally isotropic and driven by the local coefficient of thermal expansion, we also assume that the eigenstrain causing the residual stresses near the slit is isotropic and proportional to the room temperature expansion coefficient of the constituent material at a given material point.

Because we are only interested in determining the residual stresses on the plane of slitting, rather than throughout the part, we assume that the eigenstrain is driven by an unknown scalar field $T(y)$ that is only a function of *y*. In the present case, therefore, residual stress computed from the determined eigenstrain field will only be accurate on the plane of constant *x* corresponding with the slit. A similar approach was pursued previously for determining residual stress only in the bead region of a thick welded plate using sectioning [29]. More recently, a similar approach termed "initial strain" has also been used with the slitting method for rapidly varying stresses [31] and for discontinuous stresses in a layered part [32].

With these assumptions, the second-order tensor eigenstrain field ε_{kl}^* at each point in the composite is equal to the identity tensor δ_{kl} multiplied by the local room-temperature thermal expansion coefficient $\alpha(x,y)$ and the unknown scalar field $T(y)$

$$\varepsilon_{kl}^*(x,y) = \delta_{kl}\alpha(x,y)T(y)\,. \qquad (2)$$

Since the thermal expansion coefficients of the matrix and fibers are known [20], these assumptions reduce the problem of finding the eigenstrain field to determination of the univariate scalar field $T(y)$.

The unknown scalar field $T(y)$ is found by solving an elastic inverse problem using a series

expansion. We express the unknown scalar field in a polynomial basis as

$$T(y) = \sum_{j=0}^{n} A_j P_j(y) = [P]\{A\}, \qquad (3)$$

where the A_j are unknown coefficients and the basis functions $P_j(y)$ were selected as Legendre polynomials with the domain as the full thickness (y-direction) of the composite specimen. The problem of finding the scalar field $T(y)$ is therefore reduced to finding the set of n+1 unknown coefficients A_j. These coefficients are found from the strain versus depth data gathered during the slitting experiment.

To find the unknown coefficients A_j from strains measured during the slitting experiment, a linear system is formed and then inverted in a least-squares sense. As in the usual slitting application, a linear system [C] relates the unknown coefficients A_j to the strains $\varepsilon_x(a_i)$ that occur at the strain gage for slit depths a_i

$$\varepsilon_x(a_i) = \sum_{j=1}^{n} A_j C(a_i, P_j) = [C]\{A\}. \qquad (4)$$

Each member C_{ij} of the matrix [C] corresponds to the strain that would occur at a particular slit depth a_i if the eigenstrain field of Eq. 2 corresponded exactly to $T(y) = P_j(y)$. The members of [C] can be found from a series of linear elastic analyses, which compute strain ε_x at the strain gage for all combinations of slit depths and basis polynomials.

The members of [C], C_{ij}, were calculated using a finite element model. The calculations here used the commercial code ABAQUS [33]. A thermo-elastic material model was employed to introduce the eigenstrain field of Eq. 2 for each polynomial basis function $P_j(y)$ because this model was available in the commercial code and because it employs the constitutive relation of Eq. 1 when the eigenstrain is given by Eq. 2. A mesh was made to represent the composite material and had separate room temperature thermo-elastic properties for the matrix and fiber components. For a given basis function, the input to the finite element (FE) calculation was a temperature field $T(y) = P_j(y)$ (using ABAQUS user-defined subroutine `utemp.f`), which imposed the initial strain given by Eq. 2 (in usual slitting applications, the input is a normal pressure on the slit face). An equilibrium step was then taken in the analysis to calculate the thermal stresses in the absence of the slit. Next, incremental slitting was simulated by removing elements to a given depth along the path of the slit. For each polynomial basis function $P_j(y)$ and slit depth a_i, an equilibrium step was taken in the finite element code and nodal displacements were output. Displacements in the x-direction at nodes located at the boundaries of the strain gage were used with the initial gage length (distance between the nodes) to compute C_{ij}., which is the gage-averaged strain [34] corresponding to basis function $P_j(y)$ and slit depth a_i.

A 2-D finite element mesh (Fig 3, which corresponds to the side view of Fig 1) was used for the computation of the members of [C]. To reduce the effort required to build the mesh, only the relevant region of the specimen was modeled. In the central region near the slit and strain gage, a mesh of both the fibers and the matrix was constructed based on micrographs (e.g., Figure 2). Two factors dictated the choice of the boundaries of this submodel. First, the submodel extended horizontally (x) two fibers beyond the slit location and an additional fiber past the location of the strain gage. The extent of this region is more than sufficient to encompass the region where stresses will relax from the slitting because the slit was cut only to shallow depth. Second, the location of the boundaries was adjusted so that the fiber fraction in the submodel matched the 8.5 % fiber fraction for the specimen as a whole. Figure 4 shows the portion of the 2-D mesh that corresponds with Fig 2. For meshing convenience, the round-bottomed EDM slit was meshed with a square bottom. Because of the distance from the slit to the strain gage, this approximation of the slit bottom will not affect the results significantly [35]. The boundaries of the submodel were unconstrained so that the correct rigid-body rotations of the regions on each side of the slit would be calculated as the slitting and stress relaxation were simulated. Because of the large z-direction constraint provided by the wide specimen, the model assumed plane strain and used 8-node bi-quadratic generalized plane strain elements (ABAQUS type CPEG8). Generalized plane strain constrains the fiber direction (z) total strain to be constant or linear in x and y, a good assumption for a specimen prismatic and long in the z-direction. Allowing this strain to be non-zero properly admits net thermal contraction or expansion of the composite perpendicular to the modeling plane. After analysis, the resultant force from the z-direction constraint was confirmed to be zero. The elastic modulus was taken as 202 GPa, Poisson's ratio as 0.28, and the thermal expansion coefficient as 9.58×10^{-6}/C in the Kanthal matrix and 395 GPa, 0.283, and 4.40×10^{-6}/ºC in the tungsten fibers, based on previously reported room temperature properties [20].

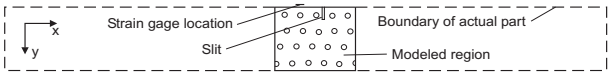

Figure 3. A submodel with the actual fiber arrangement was used for finite element calculations on the composite part. Drawing is to scale.

Given [C], a least squares fit was performed to determine the basis function amplitudes {A} which minimized the error between $\varepsilon_x(a_i)$ given by Eq. 4 and the vector of strains measured during slitting {$\varepsilon_{measured}$}

$$\{A\} = \left([C]^T[C]\right)^{-1}[C]^T\{\varepsilon_{measured}\}. \qquad (5)$$

The order of fit (i.e., n of Eq. 3) was chosen to minimize the uncertainty in the calculated stresses [15]. In order to calculate the uncertainties, it was necessary to have the slit-plane stresses corresponding to each $P_j(y)$ (Eq. 3). Those stresses were available from the FE model used to calculate [C] and were extracted after the initial

equilibrium step and before any elements were removed to simulate slitting.

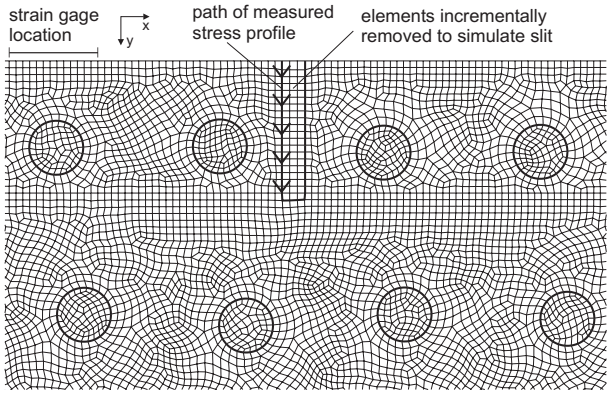

Figure 4. Finite element mesh used to calculate compliance coefficients C_{ij} and later used for predicting stresses. Figure is zoomed in on region of the mesh corresponding to Figure 2.

Given the basis function amplitudes, residual stresses on the slit plane were found by imposing $T(y)$ (Eq. 3) in a linear, thermo-elastic FE computation for the composite specimen (without a slit), using the same mesh used to calculate [C].

A more conventional analysis was used to analyze the data on the monolithic specimen. Without fibers, there was no reason to expect shear stresses on the cut plane. In fact, a calculation using eigenstrain done the same way as for the composite specimen would have given negligible shear stresses on the cut plane (identically zero for the uniform and linear $T(y)$ and for higher order terms very small away from the transverse boundaries of the specimen). Therefore, a power series with a domain from the surface to the maximum slit depth was adopted as a basis function to express the unknown normal stress on the cut plane. The members of [C] were calculated using a numerical solution [36]. Finally, the amplitudes for the power series terms were calculated using Eq. 5, and the order of the fit was chosen to minimize the estimated uncertainty.

ELASTIC-PLASTIC THERMOMECHANICAL MODEL

An elastic-plastic thermomechanical model was used to compare the measurements to a prediction based on the physical processes at work during cooling. In the analysis of the experimental data, it was assume that the eigenstrains varied only in the y-direction, which was appropriate to determine the residual stresses on the plane of the slit (i.e., at a single value of x). The actual strain field in the composite depends on x and y and is surmised to have two main sources. First, a thermoelastic strain field is expected from cooling. This strain field was represented in the data analysis by the uniform term in $T(y)$. Second, an inelastic strain field is expected to develop in the matrix during cooling, in a limited region near each fiber, due to thermoelastic property mismatch, which gives rise to strain concentration and resultant yielding. It was important to include the physical process model for comparison with the experimental measurement because the one-dimensional spatial variation of eigenstrain assumed in the data analysis differs fundamentally from these first-principle expectations.

The elastic-plastic thermomechanical model used the same material behavior as a previously published FE model of this composite [20]. However, to facilitate direct comparison with the measurements, the finite element mesh reflected the actual specimen geometry rather than using the unit cell approach previously reported. The model was a 2D analysis of the composite cross-section using generalized plane strain elements (ABAQUS type CPEG8). Material behavior was taken as elastic-perfectly plastic with von Mises yielding and temperature dependent properties. Based on *in situ* neutron diffraction measurements at various temperatures, the model used 650 ºC as a stress-free initial condition to start the analysis [20]. The cooling was assumed slow enough that the temperature was uniform throughout the specimen. Thus the temperature in the analysis was ramped from the stress-free temperature to a room temperature of 26 ºC. The temperature dependent thermal, elastic, and plastic properties were identical to those previously reported.

Only two modifications to the mesh in Figures 3 and 4 were made so that that mesh could be used for the predictive model. Unlike the calculations to analyze the slitting data, the boundaries of the submodel could not be taken as free boundaries without affecting the results. Therefore, the left edge of the modeled central region was constrained from moving in the x-direction and the right edge was constrained to remain vertical. Thus, the entire specimen was assumed be an infinite repetition of this sub-model. Unlike unit cell models, this model included the top and bottom free surfaces and the actual fiber arrangement in the region where stresses were measured.

RESULTS

Strains measured during the slitting experiment are shown in Figure 5. The gage-center to slit-edge spacing was found to be 900 μm on the monolithic specimen and 870 μm on the composite specimen. The final slit depth was 580 μm for the monolithic specimen and 490 μm for the composite specimen.

A three-term series for $T(y)$ was capable of fitting the measured strains to appropriate accuracy for the composite specimen, as was a three-term power series for $\sigma_x(y)$ for the monolithic specimen. In both specimens, an average between the three-term and four-term series solutions was used. Such averaging between successive solutions is standard practice in order to reduce endpoint instability in the solution [22]. Figure 5 shows the corresponding strain fits. Residual normal stresses σ_x were negligible in the monolithic specimen but significant in the composite specimen (Figure 6). The low stresses in the monolithic specimen increase confidence that EDM-induced stresses from slitting are not significantly affecting the results in the composite. Residual stresses predicted from the elastic-plastic FE model were extracted on the line indicated with arrows in Figure 4,

and these are compared to the slitting results in Figure 6. The slitting results on the composite closely match the shape of the FE prediction, but the FE model over predicts the stress magnitude.

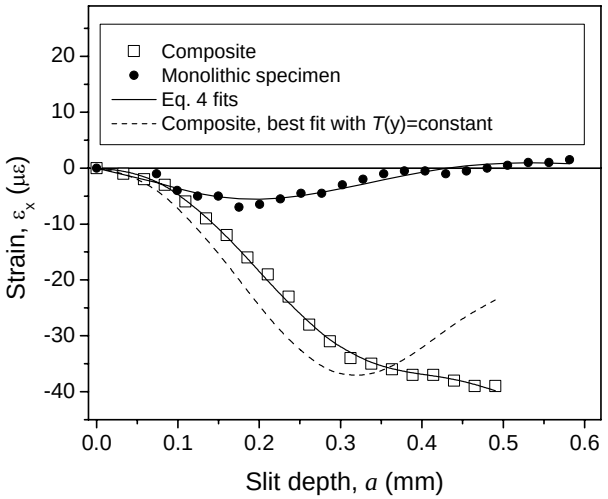

Figure 5. Strains measured during the slitting experiment (symbols) and fits to the strain data resulting from the data analysis. Constant $T(y)$, which would result from thermoelastic deformation during cooling, is not consistent with the measured strain data.

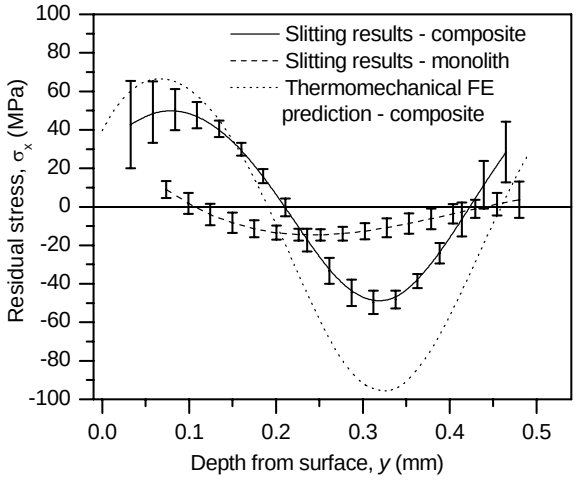

Figure 6. Depth profile of transverse residual stress (σ_x) from the slitting method in composite and monolithic specimens compared with elastic-plastic FE prediction for composite.

If residual stresses in the composite were due to only thermoelastic deformation, then the single term expansion $T(y) = A_0$ would be sufficient to fit the measured strains. The best fit for $T(y) = A_0$ is shown in Figure 5, and the poor fit quality at deep slit depths indicates that plastic deformation significantly affected the residual stresses which drive strain release during slitting. Because the plastic deformation significantly affected the residual stresses, and it is expected to have a strong spatial dependence on x (as discussed above), the measured stresses are only valid on the slit plane.

In order to facilitate further comparisons, the elastic-plastic thermomechanical model was adjusted by reducing the assumed stress free temperature in order to obtain better agreement between the measured and predicted values of σ_x. Because the model ignored viscoplastic effects, an analysis based on the experimentally determined stress free temperature could be expected to over-estimate the residual stresses. The results in Figure 6 support this contention. Neutron diffraction measurements similarly found the average stresses in the matrix of the 8.5 % V_f specimen to be lower than predicted by the model [37]. Previous studies have shown that an elastic-plastic analysis could similar results to a viscoplastic analysis if the stress-free temperature were suitably reduced [38]. Therefore, the stress-free temperature was decreased in 100 ºC increments until better agreement with the slitting results was reached at a stress-free temperature of 450 ºC.

The slitting results for all three in-plane stress components are compared with the 450 ºC model predictions in Figure 7. Considering that only the stress free temperature was adjusted in the model, the agreement for all three stress components over the whole slit depth is striking. However, improving the agreement with σ_x by making finer adjustment of the stress free temperature would result in slightly poorer agreement with the other stress components. The magnitude of the residual shear stresses τ_{xy} were about the same as the magnitude of the residual normal stress σ_x. The other normal stress, σ_y, peaks at twice the magnitude of the other components.

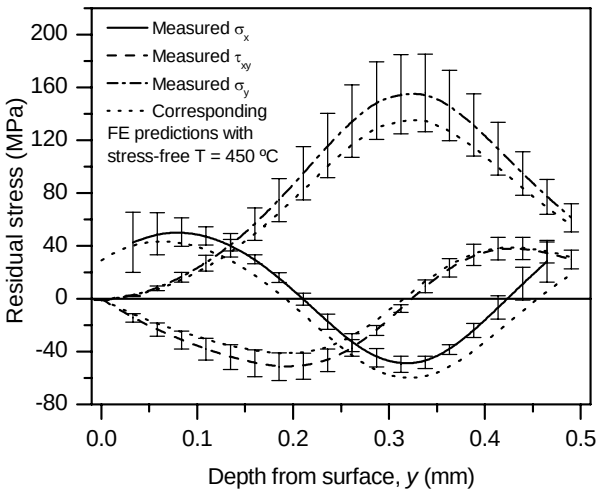

Figure 7. The slitting results for all three in-plane components of residual stress agree very well with finite element predictions.

A contour plot of the residual normal stress σ_x found from the new elastic-plastic thermomechanical model of the composite shows a complicated and spatially refined stress distribution (Figure 8). Because σ_x varies from tension to compression, an average value, as might be measured with neutrons, would give a low value and no significant information about the local stresses.

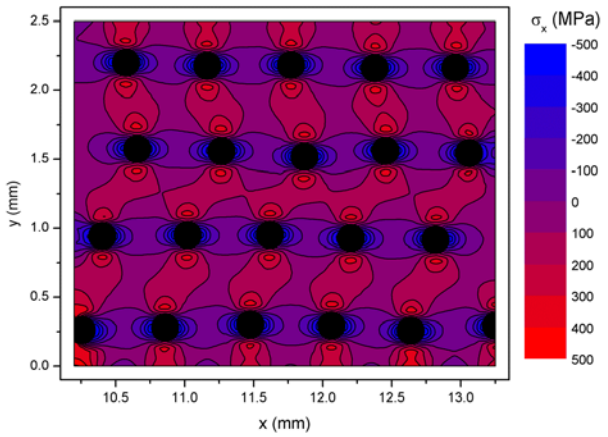

Figure 8. Contour plot of transverse residual stresses (σ_x) in matrix predicted by elastic-plastic thermomechanical FE model. The transverse stresses in the fibers, not color-coded, are relatively constant at about –500 MPa.

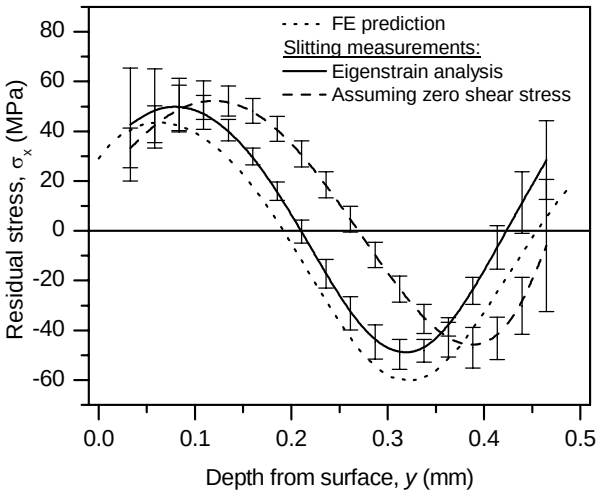

Figure 9. Incorrectly assuming the absence of shear stress on the slit plane causes significant changes from the results obtained using eigenstrain to relate shear and normal stresses.

DISCUSSION

Because of the significant shear stresses on the slit plane in the composite, the eigenstrain approach was crucial to achieving good results for this particular experiment. To illustrate this fact, the slitting data were re-analyzed using the conventional analysis technique, which assumed that shear stress was zero and that the normal stress could be expressed as a power series defined over the domain from the surface to the maximum slit depth. The compliance matrix [*C*] for this stress-based re-analysis was generated using the same FE mesh as the eigenstrain analysis, but depended on inputs of pressure on the slit face rather than a temperature field. Therefore, the only difference was in the assumptions about the nature of the stress field. Figure 9 compares the results of the eigenstrain and conventional stress-based data reductions. The plotted results for the conventional approach are the average of four-term (i.e., uniform through cubic) and five-term power series expansions, with fewer terms being insufficient to fit the data. The elastic-plastic FE prediction that assumed a 450 ºC stress-free temperature is also plotted for reference. The two data reduction methods provide the same level of peak residual stress, but the position of the stress peak is 100 μm deeper into the specimen for the stress-based data reduction. This 100 μm peak shift is about half of a fiber diameter, a quite significant distance relative to the length scale of the stress variations measured. Such errors arising from the stress-based data reduction would make it difficult to effectively compare the results of slitting to those of the elastic-plastic thermomechanical model or to use the slitting result as an experimental input to improve the model.

Using a second gage should allow one to determine the normal and shear stresses without the eigenstrain approach but would have been difficult in the test reported in this paper. A second strain gage located on the opposite side of the cut could be used to determine the normal and shear stresses in either a heterogeneous or homogeneous specimen without assuming an eigenstrain-based relationship between the stress components. Because shear stresses have approximately opposite effect on gages located on opposite sides of the slit and normal stresses have approximately equal effect, a significant shear stress effect would be recognizable in the data and the data would allow both stresses to be determined. In the test reported in this paper, installing two gages on opposite sides of the cut would have been difficult because of the small region to work in and the need to have the surface free of glue and waterproof coating, so that the small EDM wire would not break during cutting. Unlike the eigenstrain approach, the two-gage approach would work for homogeneous materials; however, homogeneous materials rarely have significant magnitudes of near-surface shear stress because of the traction-free surface condition. In the composite specimen, the subsurface shear stresses quickly build to a significant magnitude because of heterogeneity, i.e., the proximity of fibers to the surface and to the slit.

The slitting results provide a useful experimental observation that can be exploited in further refinement of the elastic-plastic thermomechanical model. As discussed previously, comparison of the initial model and experimental results indicated that the initial stress-free temperature was too high. Reduction of the stress-free temperature produced a good match with the experimental results. The temperature reduction was employed as a simple means to account for viscous stress relaxation that would occur in the material but was not included in the model. Some recent work has shown that improved predictions can be obtained by including viscoplasticity in the model [39]. Future work could be performed to

determine whether the inclusion of any of several physical phenomena (e.g., viscoplasticity, thermal gradients, strain hardening) would improve the match between model and experiment.

A significant advantage of the slitting method in these experiments is that the residual stress variation was determined on the fiber scale, and this level of spatial refinement is useful for improvement of the process model. Diffraction techniques have been used previously to determine residual stress in similar composite materials [e.g., 37], but these methods provide phase-averaged stresses over a relatively large volume. In this study, the variation of residual stress was returned on a sub-fiber scale and over a length of approximately 2.5 fiber diameters. This level of spatial refinement in the stress distribution is critical for the refinement of a numerical process model. Model improvement typically consists of certain process model variations that would affect the local distribution of residual stress on the fiber scale, and comparison of the computed stress distribution with experimental results is used to improve the model. Because slitting provides a refined spatial distribution of stress, it is an especially useful experimental technique. Phase-average stress would be less affected by model variations, so that comparison of computed and experimental average stresses is of less value in refining the process model. Any number of model variations may produce the same variations in the computed phase-average stress due to the non-uniqueness of a volume average relative to the spatial variation of the actual underlying stress field.

CONCLUSIONS

The slitting, or crack compliance, method was used to determine the fiber-scale spatial distribution of residual stress in a metal matrix composite. A significant issue with such measurements is experimentally cutting a slit between the fibers in the composite. Therefore, the reported measurements were limited to a specimen with a low volume fraction of fibers. However, the use of other methods of cutting (e.g., laser cutting) could potentially increase the applicability of the method in such materials. For example, recent work using focused ion beam machining made a slit only a few nanometers wide [40], which would allow application to composites with much smaller fibers or other applications requiring finer spatial resolution.

The eigenstrain data reduction used with the slitting data proved to be powerful and can be used with other heterogeneous specimens. The data reduction based on a simplified eigenstrain distribution allowed the determination of all the in-plane stress components, which has never been reported in the literature before with the slitting method, and the results were in good agreement with predictions from the elastic-plastic thermomechanical model. The conventional stress-based data reduction returned only a single stress component and was significantly in error due to the assumption of negligible shear stress on the slitting plane. In homogeneous specimens where shear stresses are usually small, a conventional analysis is appropriate.

The measurement of local stress variations, as compared to spatial averages, provided unprecedented comparison between measured residual stress and predictions from the process model. Where any number of stress fields might give the same average residual stresses that might be measured by a technique like layer removal or neutron diffraction, the slitting method provided a fiber-scale distribution of stress that could be directly compared to point wise values of stress from the process model.

ACKNOWLEDGEMENTS

Part of this work was performed at Los Alamos National Laboratory, operated by the University of California for the United States Department of Energy under contract W-7405-ENG-36.

REFERENCES

1 Warrier, S.G., Rangaswamy, P., Bourke, M.A.M. and Krishnamurthy, S. (1999). Assessment of the Fiber/Matrix Interface Bond Strength in Sic/Ti-6Al-4V Composites, *Materials Science and Engineering*, **A259**(2): 220-227.

2 Liu, H.Y., Zhang, X., Mai, Y.W. and Diao, X.X. (1999). On Steady-State Fibre Pull-Out - II - Computer simulation. *Composite Science and Technology*, **59**(15): 2191-2199.

3 Nath, R.B., Fenner, D.N. and Galiotis, C. (2000). The Progressional Approach to Interfacial Failure in Carbon Reinforced Composites: Elasto-Plastic Finite Element Modelling Of Interface Cracks, *Composites Part A*, **31**(9): 929-943.

4 Deve, H.E. and Maloney, M.J. (1991). On The Toughening Of Intermetallics With Ductile Fibers - Role Of Interfaces, *Acta Metallurgica et Materialia*, **39**(10), 2275-2284.

5 Nakamura, T. and Suresh, S. (1993). Effects Of Thermal Residual-Stresses And Fiber Packing On Deformation Of Metal-Matrix Composites, *Acta Metallurgica et Materialia.*, **41**(6): 1665-1681.

6 Zheng, M.H. (2000). Strength Formulae Of Unidirectional Composites Including Thermal Residual Stresses, *Maerials Letters*, **43**(1-2): 36-42.

7 Jain, L.K. and Mai, Y.W. (1996). On residual stress induced distortions during fabrication of composite shells. *Journal of Reinforced Plastics and Composites*, **15**(8): 793-805.

8 Rangaswamy, P., Prime, M.B., Daymond, M., Bourke, M.A.M., Clausen, B., Choo, H. and Jayaraman, N. (1999). Comparison of Residual Strains Measured by X-Ray and Neutron Diffraction in a Titanium (Ti-6Al-4V) Matrix Composite, *Materials Science and Engineering A*, **259**(2): 209-219.

9 Manson, J.A.E. and Seferis, J.C. (1992). Process Simulated Laminate (PSL) : A Methodology to Internal-Stress Characterization in Advanced Composite-Materials, *Journal of Composite Materials*, **26**(3): 405-431.

10 Ifju, P.G., Kilday, B.C., Niu, X.K. and Liu, S.C. (1999). A Novel Method to Measure Residual Stresses in Laminated Composites, *Journal of Composite Materials*, **33**(16): 1511-1524.

11 Withers, P.J. and Bhadeshia H.K.D.H. (2001). Residual Stress Part 2: Nature and Origins, *Materials Science and Technology*, **17**(4): 366-375.

12 Kuntz, T.A., Wadley, H.N.G. and Black, D.R. (1993). Residual Strain Gradient Determination in Metal-Matrix Composites by Synchrotron X-Ray-Energy Dispersive Diffraction, *Metallurgical Transactions A*, **24**(5): 1117-1124.
13 Korsunsky, A.M. and Wells, K.E. (2000). High Energy Synchrotron X-ray Measurements of 2D Residual Stress States in Metal Matrix Composites, *Materials Science Forum*, **321**: 218-223.
14 Hermann, R. (1995). Crack Growth and Residual Stress in Al-Li Metal Matrix Composites Under Far-Field Cyclic Compression, *Journal of Materials Science*, **30**(15): 3782–3790.
15 Hill, M.R. and Lin, W.Y. (2002). Residual Stress Measurement in a Ceramic-Metallic Graded Material, *Journal of Engineering Materials and Technology*, **124**(2): 185-191.
16 Ersoy, N. and Vardar, O. (2000). Measurement of Residual Stresses in Layered Composites by Compliance Method, *Journal of Composite Materials*, **34**(7): 575-598.
17 Kim, B.S., Bernet, N, Sunderland, P. and Manson, J.A. (2002). Numerical Analysis of the Dimensional Stability of Thermoplastic Composites Using a Thermoviscoelastic Approach, *Journal of Composite Materials*, **36**(20): 2389-2403.
18 Gungor, S. (2002). Residual Stress Measurements in Fibre Reinforced Titanium Alloy Composites, *Acta Materialia*, **50**(8): 2053-2073.
19 Titran, R. H. And Grobstein, T.L. (1990). Advanced Refractory Metals and Composites for Extraterrestrial Power Systems, *Journal of Metals*, **42**(8): 8-10.
20 Saigal, A. and Leisk G.G. (1997). Residual Strains and Stresses in Tungsten/Kanthal Composites, *Materials Science and Engineering*, **A237**(1): 65-71.
21 Klopp, W.D., Witzke W.R. and Raffo, P.L. (1965). Effects of Grain Size on Tensile and Creep Properties of Arc-Melted and Electron-Beam-Melted Tungsten at 2250° to 4140°F, *Transactions of the Metallurgical Society of AIME*, **233**(10): 1860-1866.
22 Prime, M.B. (1999). Residual Stress Measurement by Successive Extension of a Slot: The Crack Compliance Method, *Appl. Mech. Rev.*, **52**(2): 75-96.
23 Cheng, W., Finnie, I., Gremaud, M., Rosselet, A. and Streit, R.D. (1994). The Compliance Method for Measurement of Near Surface Residual Stresses - Application and Validation for Surface Treatment by Laser and Shot-Peening, *Journal of Engineering Materials and Technology*, **116**(4): 556-560.
24 Rankin, J.E., Hill, M.R. and Hackel, L.A. (2003). The Effects Of Process Variations On Residual Stress In Laser Peened 7049 T73 Aluminum Alloy, *Materials Science And Engineering A*, **A349**(1-2): 279-291.
25 Cheng, W., Finnie, I., Gremaud, M. and Prime, M.B. (1994). Measurement of Near Surface Residual Stresses Using Electric Discharge Wire Machining, *Journal of Engineering Materials And Technology*, **116**(1): 1–7.
26 Schajer, G.S. (1981). Application of Finite-Element Calculations to Residual-Stress Measurements, *Journal of Engineering Materials And Technology*, **103**(2): 157-163.
27 Ueda, Y. and Fukuda, K. (1989). New Measuring Method of Three-Dimensional Residual Stresses in Long Welded Joints Using Inherent Strains As Parameters-L_z Method, *Journal of Engineering Materials and Technology*, **111**(1): 1-8.
28 Hill, M.R. (1996). *Determination of Residual Stress Based on the Estimation of Eigenstrain*, PhD Dissertation, Stanford University.
29 Hill, M.R. and Nelson, D.V. (1998). The Localized Eigenstrain Method for Determination of Triaxial Residual Stress in Welds, *PVP* **373**: 397-403, ASME, New York.
30 Mura, T. (1991). *Micromechanics of defects in solids*, Kluwer Academic Publishers, Boston, MA.
31 Cheng, W. (2000). Measurement of the Axial Residual Stresses Using The Initial Strain Approach, *Journal Of Engineering Materials And Technology*, **122**(1): 135–140.
32 Cheng, W., Finnie, I. and Ritchie, R. (2001). Residual Stress Measurement on a Pyrolytic Carbon-Coated Graphite Leaflet, Proc. 2001 SEM Annual Conference on Experimental and Applied Mechanics, June 4-6, Portland, Oregon, 604-607.
33 ABAQUS/Standard User's Manual Version 6.2. Hibbitt, Karlsson & Sorensen, Inc., Pawtucket, Rhode Island, USA (2001).
34 Schajer, G.S. (1993). Use of Displacement Data to Calculate Strain Gauge Response in Non-Uniform Strain Fields, *Strain*, **29**(1): 9-13.
35 Nowell, D. (1999). Strain Changes Caused by Finite Width Slots, with Particular Reference to Residual Stress Measurement, *Journal of Strain Analysis for Engineering Design*, **34**(4): 285-294.
36 Cheng, W., Finnie, I. (1993). A Comparison of the Strains Due to Edge Cracks and Cuts of Finite Width with Applications to Residual-Stress Measurement, *Journal Of Engineering Materials And Technology*, **115**(2): 220–226.
37 Rangaswamy, P., Beyerlein I.J., Bourke M.A.M., Prime M.B., Saigal A.K. and Williams T.O. (2003). Residual Stresses in Continuous-Tungsten-Fiber-Reinforced Kanthal-Matrix Composites, *Philosophical Magazine*, **83**(19): 2267-2292.
38 Kroupa, J.L. and Neu, RW (1994). The Nonisothermal Viscoplastic Behavior Of A Titanium-Matrix Composite. *Composites Engineering*. **4**(9): 965-977.
39 Choo, H., Bourke, M.A.M. and Daymond, M.R. (2001). A Finite-Element Analysis of the Inelastic Relaxation of Thermal Residual Stress in Continuous-Fiber-Reinforced Composites, *Composites Science And Technology*, **61**(12): 1757-1772.
40 Kang, K.J., Yao, N., He, M.Y. and Evans, A.G. (2003). A Method for in Situ Measurement of the Residual Stress in Thin Films by Using the Focused Ion Beam, *Thin Solid Films*, **443**(1-2): 71–77.